Shift of the Na I 467- and 498-nm lines in a dense plasma

M. Kettlitz and P. Oltmanns
Institut für Niedertemperatur-Plasmaphysik e.V. an der Ernst-Moritz-Arndt-Universität Greifswald, Robert-Blum-Straße 8-10, D-17489 Greifswald, Germany
(Received 9 May 1996; revised manuscript received 13 August 1996)

The shifts of the Na I 467- and 498-nm lines were measured and calculated as a function of the electron density at a temperature of 4000 K and at electron densities around 10^{16} cm^{-3}. It is shown that even at these small electron densities collective effects such as plasma oscillations lead to dramatic changes in Stark line shifts as compared to those calculated in the binary collision approximation. Therefore a multiparticle theory is used to describe the relevant processes in order to analyze the experimental data. The Green's function approach used in this paper has been shown to take all the relevant multiparticle effects correctly into account. We show that the line shifts are caused by the levels closely adjacent to the initial level of the radiating atom. As a consequence of the plasma oscillations the line shift is screened off when the plasma frequency reaches the order of magnitude of the energy difference between the radiating and the adjacent levels. [S1063-651X(96)03412-5]

PACS number(s): 52.40.−w, 32.60.+i, 32.70.Jz

I. INTRODUCTION

Stark broadening of spectral lines provides a valuable tool for investigations in the field of plasma physics. At low electron densities line shifts due to the quadratic Stark effect are proportional to the electron density. Many experiments [1–7] in dense plasmas have shown deviations from this linear behavior. In most cases these effects became visible at electron densities around 10^{18} cm^{-3}. In this paper we treat transitions where such a behavior occurs at far lower densities. A wide range of theoretical investigations has been performed in the last decades starting with a model of classical perturbers (see, for example, Refs. [8,9]). Afterwards quantum-mechanical approaches were also used both in relaxation theories [10,11] and in formalisms using Green's function techniques [12–16]. The continuing interest in this field is demonstrated also by further improvements of the theoretical situation (see, for example, [17–22]).

II. THEORY

The theory used to interpret our experiment has been thoroughly introduced (see Refs. [21–23]). The shift of the lines considered here is to a great extent caused by the quadratic Stark effect. The main contribution is caused by perturbing electrons in the plasma, a minor one also by ions. Due to the different masses and therefore different velocities their contributions to the shift are calculated separately. A Green's function technique has been used to investigate the effect of the perturbing electrons taking into account many-particle effects. A relation between the absorbed radiation and the Green's function serves as a starting point for this approach. This relation can be obtained by investigating the linear reaction of a system on an external field and using Fermi's golden rule. The polarization function plays an important role in this relation, and is calculated in a perturbative expansion which is carried out using a diagram technique. The following approximations have been used: (i) a three-particle-impulse approximation, which is evaluated up to (with respect to particle densities) linear contributions; (ii) restriction to the treatment of isolated lines, i.e., no profile overlaps; and (iii) introduction of the impact limit, i.e., the description of the line shape only close to the unperturbed transition frequency.

It can be shown that in the classical limit the resulting formulas reduce to those of the model of classical perturbers. Taking into account only levels that are closely adjacent to the initial state, this approach coincides with the kinetic theory.

The line shift caused by perturbing electrons is given by

$$d^{(e)}=\delta_i-\delta_f, \tag{1}$$

where δ_n is given by

$$\delta_n=-\sum_\alpha \int \frac{d\vec{k}}{(2\pi)^3}V(\vec{k})\int_{-\infty}^{\infty}\frac{d\omega}{\pi}\mathrm{Im}\epsilon^{-1}(\vec{k},\omega+i0) \times[1+n_B(\omega)]\frac{|M_{n\alpha}(\vec{k})|^2}{E_n-E_\alpha-(\omega+i0)} \tag{2}$$

and $M_{n\alpha}$ by

$$M_{n\alpha}(\vec{k})=i\int\frac{d\vec{p}}{(2\pi)^3}\Psi_n^*(\vec{p})[\Psi_\alpha(\vec{p})-\Psi_\alpha(\vec{p}+\vec{k})]. \tag{3}$$

The states closely adjacent to n are denoted by α, and the wave functions (of the states n and α) Ψ_n and Ψ_α are calculated using the Coulomb approximation. As we investigate the line shifts at electron densities around 10^{16} cm^{-3} and at temperatures of only a few tenths of an eV, the Fermi distribution f_e can be approximated by the Boltzmann distribution. Moreover, only the leading term in electron densities has to be taken into account, so that δ_n is given by

$$\delta_n=-\frac{8}{\pi}\left(\frac{\beta}{\pi}\right)^{1/2}n_e\sum_\alpha\int\frac{d\vec{k}}{k^4}|M_{n\alpha}(\vec{k})|^2 I(k,\omega_{\alpha n}), \tag{4}$$

where $\omega_{\alpha n}$ denotes the energy difference between the state n and the adjacent state α. β denotes the inverse temperature $(k_B T)^{-1}$, and I $(k,\omega_{\alpha n})$, which is responsible for dynamic screening, is represented with the help of the dielectric function ϵ by

$$I(k,\omega_{\alpha n})=\int_{-\infty}^{\infty} dp e^{-\beta p^2}\frac{|\epsilon(k,k^2-2pk+i0)|^2}{\omega_{\alpha n}-2pk+k^2+i0}. \quad (5)$$

The dielectric function can be represented in random-phase approximation (RPA) as

$$\epsilon(\vec{k},\omega)=1-2\int \frac{d\vec{p}}{(2\pi)^3}V(k)\frac{f_e(E_{\vec{p}})-f_e(E_{\vec{p}-\vec{k}})}{E_{\vec{p}}-E_{\vec{p}-\vec{k}}-\omega}. \quad (6)$$

Its real and imaginary parts can be evaluated as

$$\mathrm{Re}\epsilon(\vec{k},\omega)=1+\frac{8\pi\sqrt{\beta}n_e}{k^3}[F(x)-F(y)] \quad (7)$$

and

$$\mathrm{Im}\epsilon(\vec{k},\omega)=\frac{4\sqrt{\pi^3\beta}n_e}{k^3}e^{-x^2}(e^{\beta\omega}-1), \quad (8)$$

where $F(x)$ represents the Dawson integral

$$F(x)=e^{-x^2}\int_0^x e^{t^2}dt, \quad (9)$$

and x and y are given by

$$x=\frac{\sqrt{\beta}}{2}\left(\frac{\omega}{k}+k\right), \quad (10)$$

$$y=\frac{\sqrt{\beta}}{2}\left(\frac{\omega}{k}-k\right). \quad (11)$$

For the interpretation of the results the model as described above is compared with the binary collision approximation (BCA), which can be obtained by setting $|\epsilon|^2=0$. This approximation does not take multiparticle correlations into account.

For a comparison with the experimental data, the ion contribution to the shift has to be included in the calculation. Following Griem [24], we calculate the full line shape as a convolution of electron impact profiles with quasistatic quadratic Stark effect profiles for the ion broadening

$$I(\omega)=\frac{w}{\pi}\int_0^\infty dF\, W(F)\frac{w^{(e)}}{(\omega-\omega_0-d^{(e)}-CF^2)^2+(w^{(e)})^2}. \quad (12)$$

Here ω_0 is the unperturbed frequency, the width is denoted by $w^{(e)}$, and *W(F)* is the microfield distribution. We have chosen the microfield distribution according to the calculations of Hooper [25].

The Stark coefficient C can be obtained by the relation

$$A=\left(\frac{CF_0^2}{w^{(e)}}\right)^{3/4}, \quad (13)$$

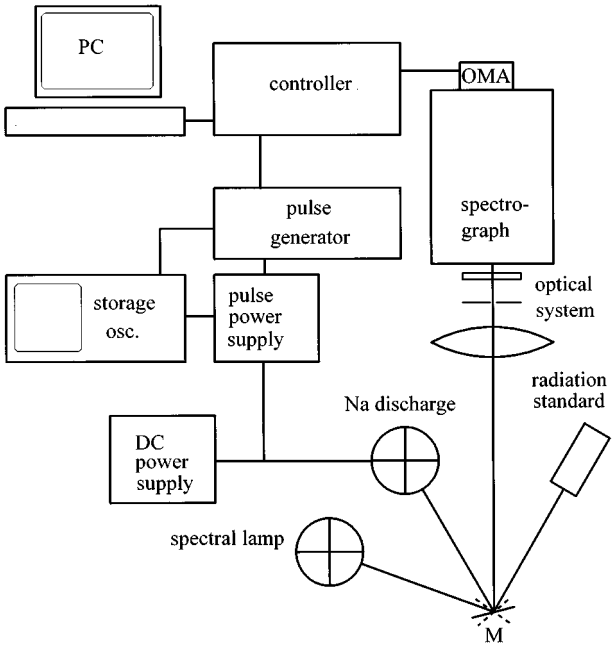

FIG. 1. Experimental setup.

where F_0 is the (normal) Holtsmark field strength, and the values for A are taken from [24].

III. EXPERIMENT

A schematic diagram of the experimental arrangement is given in Fig. 1. The experiments are performed in electrical wall-stabilized pulse discharges. Due to the extreme aggressive chemical behavior of hot alkali vapors the cylindrical discharge tube consists of sapphire. It is 7.6 cm long and has an inner diameter of 0.48 cm. The electrodes are made of tungsten. The tube contains some milligrams of sodium and a small amount of argon as an ignition gas. A special technique and handling are applied to prepare and seal the discharge tube. Finally the tube is mounted in an evacuated glass bulb.

The discharge is operated in a so-called simmer mode that keeps the plasma in the conducting state by means of a dc discharge [26]. The dc power input controls the cold-spot temperature in the discharge tube and therefore the available alkali vapor pressure. With a second circuit high current, pulses are added. A pulse shaping circuit consisting of six capacitors and inductance coils is used to form nearly rectangular current pulses with a duration of 1 ms. The electrical pulses are switched by a thyristor from the capacitors into the low current dc discharge. The stationary dc power is about 50 W. It is superimposed by current pulses with values from 1 A up to 40 A, and hence a maximum power input of up to 5 kW is reached. During the pulse regime, plasma temperature and particle number densities and hence the optical output are determined by the pulse power.

The spectroscopic measurements are performed during the pulse current plateau in the visible and near infrared spectral range. The radiation of the discharge passes an optical mirror system and is imaged to the entrance slit of a 0.5-m spectrograph. The side-on intensity distribution is re-

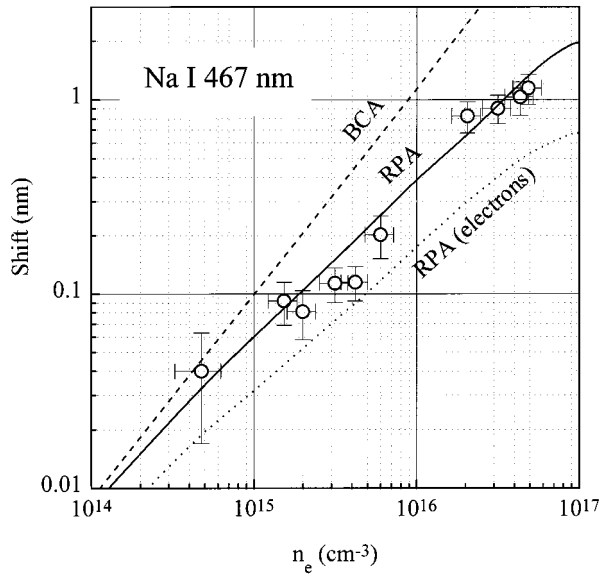

FIG. 2. Wavelength shift of the Na I 467-nm line as a function of the electron density: (o) measurement; (- -) BCA; (–) RPA; and (· ·) RPA electron contributions.

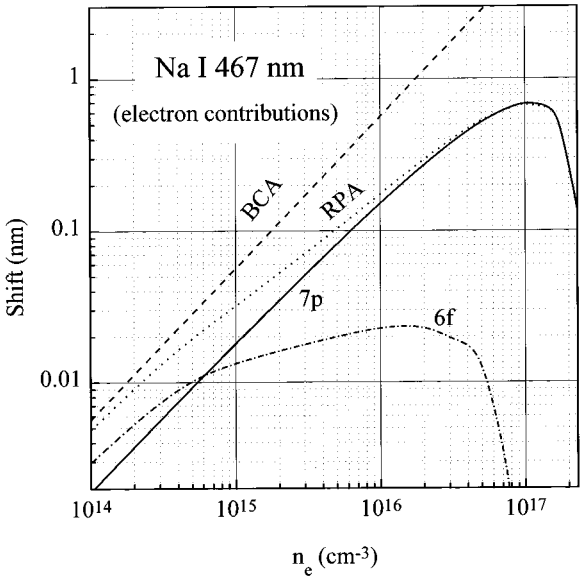

FIG. 3. Electron contributions to the wavelength shift of the Na I 467-nm line as a function of the electron density.

corded with different gratings. For the shift measurements a grating of 1800 groves/mm with a resolution of 0.023 nm is used. The data are recorded by means of a gated optical multichannel analyzer (OMA) system connected to a computer for further processing of the images. For an absolute radiation calibration a xenon radiation standard [27] is used. Wavelength calibration of the spectrometer is provided by low pressure sodium and mercury spectral lamps for the different spectral ranges. The radial line profiles of the Stark broadened sodium lines at 467, 475, and 498 nm are measured. The radial distribution in the plasma is obtained by Abel inversion based on the principle of Fourier analysis [28]. Only the data of the discharge axis are taken into account in order to determine the line shifts. Then the measured spectra are fitted with calculated spectra of the lines occurring in that spectral region using Lorentz profiles. The line shifts are determined from the difference of the centers of the fitted lines to their unshifted position.

The electron densities in the discharge axis are derived from the data of the Na I line at 475 nm ($7s$-$3p$) with the Stark broadening parameters calculated by Dimitrijevic [29,30]. RPA calculations confirm these values. Finally in the experiment electron densities between 5×10^{14} and 7×10^{16} cm^{-3} are reached in the discharge axis. The plasma temperatures are derived from the absolute intensities of the 467- and 498-nm lines [32], taking the atomic data from Wiese [31]. Thus the temperatures in the discharge axis are between 3000 and 4500 K.

IV. RESULTS AND DISCUSSION

In Fig. 2 the calculated and measured line shift of the Na I line at 467 nm ($6d$-$3p$) is plotted as a function of the electron density. The calculations including dynamic screening (full curve) are compared with the one using the binary collision approximation (dashed curve). There is quite a good agreement of the results with dynamic screening with the experimental data over the whole range of electron density. There is, however, an increasing discrepancy to the BCA results. At electron densities of 10^{16} cm^{-3} the BCA results are too large by a factor of 2. Landen *et al.* [36] performed experiments in resonantly pumped sodium vapor. They found shift values of 1.5 nm for electron densities of 10^{16} cm^{-3}, which are smaller than our values.

In addition to the total line shift the electron contributions to the shift are shown (dotted curve). These electron contributions originate from the two levels closely adjacent to the $6d$ level, i.e., the $7p$ and $6f$ levels, which have energy differences from the $6d$ level of 0.019 and 0.002 eV, respectively. These two levels lead to shift contributions which are proportional to the electron density in case of low electron densities. Due to the dynamically screened electron-atom interaction, these contributions deviate from their proportionality and finally fall with increasing electron densities when the plasma frequency reaches the same order of magnitude as the energy difference between the corresponding level and the $6d$ level. These electron contributions are plotted separately in Fig. 3. At an electron density of 3×10^{14} cm^{-3} the $6f$ contribution (dash-dotted curve) deviates from the linearity. This contribution already reaches its maximum value at 10^{15} cm^{-3}. For higher densities the shift is dominated by the $7p$ contribution (full curve). At 10^{16} cm^{-3} the $7p$ contribution is already larger by an order of magnitude than the one originating from the $6f$ level. On the other hand, according to the BCA the shift is always dominated by the $6f$ level, and therefore is in complete disagreement with our calculation that takes into account the dynamically screened potential. The reason for this behavior is that for small electron densities the electron impact is directed on the optical electron, whereas with increasing densities it becomes attracted by the surrounded plasma, resulting in spatial and temporal plasma oscillations. These results are consistent with previous ones obtained for xenon and cesium lines [33–35].

The contributions to the shift caused by the ions can be

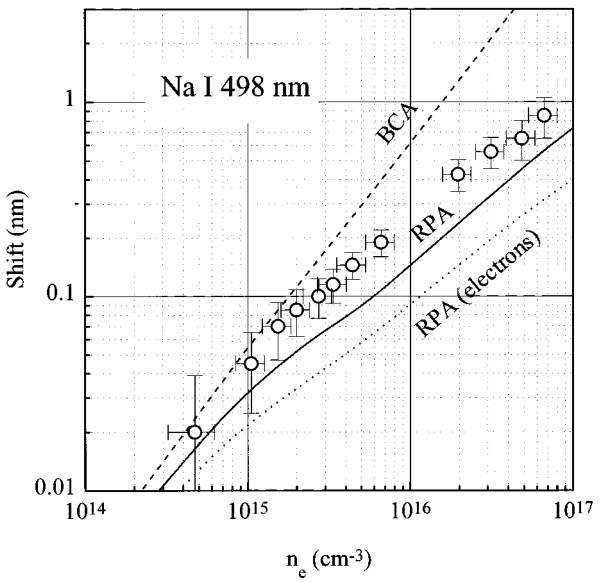

FIG. 4. Wavelength shift of the Na I 498-nm line as a function of the electron density: (o) measurement; (- -) BCA; (–) RPA; and (· ·) RPA electron contributions.

treated in the quasistatic approximation, as previously described. For the line considered here, the effect of the ions is about as strong as that of the electrons, and its relative magnitude rises with increasing electron densities. Although there is an almost proportional relationship between the total (combined electron and ion produced) line shift and the electron density, these shifts are still considerably smaller than the BCA shifts produced by electrons only for electron densities above 10^{16} cm^{-3}.

In Fig. 4 an analogous plot for the 498-nm ($5d$-$3p$) line is shown. The result is similar to the one obtained for the $6d$-$3p$ line. Now the energy differences of the $6d$ level from the $6p$ and $5f$ levels are 0.002 and 0.031 eV, respectively. That is why the effect of dynamic screening starts at somewhat higher densities (and thus higher plasma frequencies). For the 467-nm line the energy differences of the $7p$ and $6f$ levels correspond to electron densities of 2.6×10^{17} and 1.9×10^{15} cm^{-3}, respectively, whereas the corresponding values for the $6p$ and $5f$ levels for the 498-nm line are 7.5×10^{17} and 4.8×10^{15} cm^{-3}, respectively. In both figures it can be seen that at these values the contributions caused by these levels to the total line shift are completely screened off.

The reason why the 475-nm line can be used to measure the electron density in our experiment can be explained in the following way: The two main contributions to that line shift, i.e., the $7p$ and $6p$ levels, lead to line shifts of opposite sign. The energy differences to the $7s$ level are -0.085 and 0.062 eV, respectively. So both contributions are only weaker subjected to the effect of dynamic screening. Moreover, as the screening of both contributions is similar, the screening of one contribution is compensated for by the other one. Therefore their sum is almost linear with respect to the electron density, so that it is well suited to measure the electron density.

ACKNOWLEDGMENT

The authors are grateful to Jim Dufty for helpful discussions and comments.

[1] H. Hess, Contrib. Plasma Phys. **26**, 209 (1986).
[2] V. E. Fortov, V. E. Bespalov, M. I. Kulish, and S. I. Kuz, in *Strongly Coupled Plasma Physics*, edited by S. Ichimaru (Elsevier, Yamada, 1990), p. 571.
[3] St. Böddeker, S. Günter, A. Könies, L. Hitzschke, and H.-J. Kunze, Phys. Rev. E **47**, 2785 (1993).
[4] N. I. Uzelac and N. Konjevic, J. Phys. B **22**, 2517 (1989).
[5] D. J. Heading, J. P. Marangos, and D. D. Burgess, J. Phys. B **25**, 4745 (1992).
[6] M. Kettlitz, R. Radtke, R. Spanke, and L. Hitzschke, J. Quantum Spectrosc. Radiat. Trans. **34**, 275 (1985).
[7] M. Kettlitz and R. Radtke, in *Teubner-Texte zur Physik*, edited by W. Ebeling, A. Förster, and R. Radtke (Teubner, Lepzig, 1992), Vol. 26, p. 233.
[8] H. R. Griem, M. Baranger, A. C. Kolb, and G. K. Oertel, Phys. Rev. **125**, 177 (1962).
[9] H. R. Griem, *Plasma Spectroscopy* (McGraw-Hill, New York, 1964).
[10] E. W. Smith and C. F. Hooper, Phys. Rev. **157**, 126 (1967).
[11] D. Voslamber, Phys. Lett. A **40**, 266 (1972).
[12] L. Klein, J. Quantum Spectrosc. Radiat. Trans. **9**, 199 (1969).
[13] H. R. Zaidi, Phys. Rev. **173**, 123 (1968).
[14] H. R. Zaidi, Phys. Rev. **173**, 132 (1968).
[15] D. W. Ross, Ann. Phys. **36**, 458 (1966).
[16] M. W. C. Dharma-wardana, F. Grimaldi, A. Lecourt, and J. L. Pellisier, Phys. Rev. A **21**, 379 (1980).
[17] W. D. Kraeft, W. Ebeling, and G. Röpke, *Quantum Statistics of Charged Particle Systems* (Akademie-Verlag, Berlin, 1986).
[18] T. Hussey, J. W. Dufty, and C. F. Hooper, Phys. Rev. A **12**, 1084 (1975).
[19] C. A. Iglesias and J. W. Dufty, in *Spectral Line Shapes II*, edited by K. Burnett (de Gruyter, Berlin, 1984), p. 55.
[20] E. Oks, A. Derevianko, and Ya. Ispolatov, J. Q. S. R. T. **54**, 307 (1995).
[21] S. Günter, L. Hitzschke, and G. Röpke, Phys. Rev. A **44**, 6834 (1991).
[22] L. Hitzschke, G. Röpke, T. Seifert, and R. Zimmermann, J. Phys. B **19**, 2443 (1986).
[23] L. Hitzschke, Ph. D. thesis, Humboldt Universität Berlin, 1987.
[24] H. R. Griem, *Spectral Line Broadening in Plasmas* (Academic, New York, 1974).
[25] C. F. Hooper, Phys. Rev. **165**, 215 (1968).
[26] K. Guenther and R. Radtke, *Electric Properties of Weakly Nonideal Plasmas* (Birkhäuser, Basel, 1984).
[27] K. Guenther and R. Radtke, J. Phys. E **8**, 371 (1975).
[28] G. Pretzler, Z. Naturforsch. **46a**, 639 (1991).
[29] M. S. Dimitrijevic and S. Sahal-Brechot, J. Q. S. R. T. **44**, 421 (1990).

[30] M. S. Dimitrijevic and S. Sahal-Brechot, Bull. Obs. Astron. Belgrade **142**, 59 (1990).
[31] W. L. Wiese, M. W. Smith, and B. M. Miles, Atomic Transition Probabilities Vol. II. NSRDS-NBS 22, National Stand. Ref. Data Ser., National Bureau of Standards, Washington (1969).
[32] J. J. de Groot and J. A. J. M. van Vliet, *The High-Pressure Sodium Lamp* (Kluwer, Deventer, 1986).
[33] L. Hitzschke, in *Teubner-Texte zur Physik*, edited by W. Ebeling, A. Förster, and R. Radtke (Teubner, Leipzig, 1992), Vol. 26, p. 225.
[34] L. Hitzschke and S. Günter, J. Quantum Spectrosc. Radiat. Trans. **56**, 423 (1996).
[35] M. Kettlitz, Ph. D. thesis, Humboldt Universität Berlin, 1993 (unpublished).
[36] O. L. Landen, R. J. Winfield, D. D. Burgess, and J. D. Kilkenny, Phys. Rev. A **32**, 2963 (1985).